Title: Subcellular localisation of Theiler's Murine Encephalomyelitis Virus (TMEV) capsid subunit VP1 vis-á-vis host protein Hsp90

Author: Caroline Ross Nicole Upfold Garry A. Luke Özlem Tastan Bishop Caroline Knox

PII: S0168-1702(16)30279-9
DOI: http://dx.doi.org/doi:10.1016/j.virusres.2016.06.003
Reference: VIRUS 96898

To appear in: *Virus Research*

Received date: 5-5-2016
Revised date: 30-5-2016
Accepted date: 2-6-2016

Please cite this article as: Ross, Caroline, Upfold, Nicole, Luke, Garry A., Bishop, Özlem Tastan, Knox, Caroline, Subcellular localisation of Theiler's Murine Encephalomyelitis Virus (TMEV) capsid subunit VP1 vis-á-vis host protein Hsp90.Virus Research http://dx.doi.org/10.1016/j.virusres.2016.06.003

Subcellular localisation of Theiler's Murine Encephalomyelitis Virus (TMEV) capsid subunit VP1 vis-á-vis host protein Hsp90

Caroline Ross[a#], Nicole Upfold[b#], Garry A. Luke[c], Özlem Tastan Bishop[a], Caroline Knox[b*]

[a]Research Unit in Bioinformatics (RUBi), Department of Biochemistry and Microbiology, Rhodes University, Grahamstown, 6140, South Africa

[b]Department of Biochemistry and Microbiology, Rhodes University, Grahamstown 6140, South Africa

[c]Centre for Biomolecular Sciences, School of Biology, Biomolecular Sciences Building, University of St Andrews, North Haugh, St Andrews, Scotland KY16 9ST, UK

[*]Correspondence to Caroline Knox; E-mail: caroline.knox@ru.ac.za

[#]These authors contributed equally to this article.

Highlights

- TMEV VP1 localises to the perinuclear region and cytoplasm of infected cells
- TMEV VP1 and Hsp90 colocalise in the perinuclear region and cytoplasm
- TMEV VP1 did not localise to the nucleus during infection
- A typical NLS was absent from the TMEV VP1 sequence
- TMEV VP1 localises in a similar manner to FMDV and EV71 VP1

Abstract

The VP1 subunit of the picornavirus capsid is the major antigenic determinant and mediates host cell attachment and virus entry. To investigate the localisation of Theiler's murine encephalomyelitis virus (TMEV) VP1 during infection, a bioinformatics approach was used to predict a surface-exposed, linear epitope region of the protein for subsequent expression and purification. This region, comprising the N-terminal 112 amino acids of the protein, was then used for rabbit immunisation, and the resultant polyclonal antibodies were able to recognise full length VP1 in infected cell lysates by Western blot. Following optimisation, the antibodies were used to investigate the localisation of VP1 in relation to Hsp90 in infected cells by indirect immunofluorescence and confocal microscopy. At 5 hours post infection, VP1 was distributed diffusely in the cytoplasm with strong perinuclear staining but was absent from the nucleus of all cells analysed. Dual-label immunofluorescence using anti-TMEV VP1 and anti-Hsp90 antibodies indicated that the distribution of both proteins colocalised in the cytoplasm and perinuclear region of infected cells. This is the first report describing the localisation of TMEV VP1 in infected cells, and the antibodies produced provide a valuable tool for investigating the poorly understood mechanisms underlying the early steps of picornavirus assembly.

Keywords: Theiler's murine encephalomyelitis virus, VP1, Hsp90, Polyclonal antibody, Capsid

1. Introduction

Picornaviruses are a diverse family of small non-enveloped RNA viruses that includes various pathogens of significant clinical and economic importance. Notable human pathogens include poliovirus (PV), human rhinovirus (HRV), Coxsackievirus A and B (CVA; CVB), enterovirus 71 (EV71) and hepatitis A virus (HAV) (Hagan et al., 2015; Rotbart and Hayden, 2000). Animal pathogens of high economic importance include foot-and-mouth disease virus (FMDV) and swine vesicular disease virus (SVDV) (Brito et al., 2015; Mansour et al., 2015).

The picornavirus capsid is a non-enveloped icosahedral capsid with pseudo-T = 3 symmetry and is approximately 30 nm in diameter. The capsid consists of 60 capsomers each of which contains three subunits, namely VP1, VP2 and VP3. A fourth capsid protein, VP4, is found on the internal side of the capsid (Bedard and Semler, 2004). Picornavirus capsids exemplify macromolecule assembly through the consecutive oligomerisation of different protein complexes (Fig. 1). Following the cleavage of the precursor P1, the subunits assemble into protomer structures, each comprising a single copy of the VP0, VP1 and VP3 subunits. The pentamer structures are subsequently formed through the interaction of five protomer structures. Formation of 80S empty procapsids then occurs following the assembly of 12 pentamer structures. Alternatively 12 pentamers assemble around the mRNA genome to constitute the 150S provirion, and cleavage of the VP0 precursor yields mature infectious virus particles (Jiang et al., 2014).

The most external and accessible surface protein of the capsid is VP1. The general structure of the protein is wedge shaped and consists of eight stranded β-barrels, with connecting loops between the barrels and the N and C termini of the protein (Rueckert, 1996). VP1 has been reported to play a role in host cell attachment, and is considered the most immunodominant of the four capsid proteins (Edlmayr et al., 2011; Meloen Briaire et al., 1983; Rossmann et al., 1985). There have been several investigations into the identification of immunogenic regions within this protein. In FMDV, the VP1 capsid protein has been reported to contain the highest number of neutralisation sites, particularly within the βG-βH loop region (Collen et al., 1991). Varrasso et al., (2001) identified neutralisation sites located within the N and C termini as well as the βE-βF and βG-βH loops of Equine Rhinitis Virus (ERAV) VP1, with strong antibody recognition against the N-terminus. Similarly, major VP1 neutralisation sites have been reported for TMEV (Cameron et al., 2001; Luo et al., 1992) and the enteroviruses

(Mateu, 1995; Oberste et al., 1999; Wu et al., 2001) with key neutralising determinants located in the N-terminal region of VP1 (Bobek et al., 2010; Tan and Cardosa, 2007) .

Since picornavirus genomes have limited coding capacity, these viruses are dependent on a range of host cellular proteins and pathways to mediate viral entry, replication and assembly. While it has been established that pentamers self-assemble into intact empty capsids *in vitro* in a process mediated by protein-protein interactions with no apparent requirement for other viral or cellular factors (Li et al., 2012; Rombaut et al., 1991), the steps between P1 to pentamer assembly are complex, and appear to involve multiple viral and cellular components. Significantly, it has been established that chaperones in the heat shock protein family, for example Hsp90 and Hsp70, are crucial for enterovirus replication as indicated by an association of these chaperones with the capsid P1 precursor (Geller et al., 2007; Macejak and Sarnow, 1992). While strong evidence links the involvement of Hsp90 in P1 processing, it has also been reported that Hsp90 promotes the formation of pentamers from 5S protomers during FMDV infection (as reviewed by Jiang et al., 2014).

To date, most studies investigating picornavirus replication and assembly have been carried out using picornaviruses such as PV, HAV and FMDV. Very few describe the localisation of picornavirus capsid subunits in cells at the early stages of virus assembly, which remains a poorly understood process in the virus life cycle. Theiler's murine encephalomyelitis virus (TMEV) is a naturally occurring murine Cardiovirus infecting the central nervous system of mice causing demyelination (Lipton, 1975). Several strains of the virus have been identified with the GDVII and FA strains being highly neurovirulent and causing acute fatal encephalitis in mice. The BeAn and DA strains are less virulent inducing a chronic demyelinating condition, and these have been extensively studied as a model for investigating the pathogenesis of multiple sclerosis (reviewed by Oleszak et al., 2004). Furthermore, the capsid structure of the TMEV DA strain has been determined at atomic resolution using X-ray crystallography providing a template on which other strains can be modelled (Grant et al., 1992). Our previous studies have reported that the TMEV GDVII 2C protein localises to the Golgi apparatus and endoplasmic reticulum (ER) both during infection, and when expressed alone in cells (Jauka et al., 2010; Murray et al., 2009). In addition, we have reported that TMEV infection results in a redistribution of Hsp90 into the replication complex where it overlaps with viral replication protein 2C, and that inhibition of Hsp90 by geldanamycin and novobiocin supresses the cytopathic effect of the virus suggesting an important role for this protein in the virus life cycle (Mutsvunguma et al., 2011). To extend these studies and further investigate virus-host interactions during infection, we used a bioinformatics approach to

analyse the nucleotide sequence of the VP1 capsid subunit and predict a potential antigenic region. The peptide consisting of amino acids 1-112 in frame with a 6x histidine tag was successfully expressed in *Escherichia coli* cells, solubilised in the presence of N-Lauroylsarcosine and purified for subsequent immunisation of rabbits. The antibodies were used to investigate the localisation of VP1 at 5 hours post infection (hpi) and determine the distribution of VP1 relative to Hsp90.

2. Materials and Methods

2.1 Homology modelling of the TMEV GDVII protomer complex

2.1.1 Sequence retrieval, alignment and template selection

The protein sequences, corresponding to the four subunits of the TMEV GDVII protomer were retrieved from the GenBank database (NCBI VP1-VP4: NP_740427.1, NP_740425.1, NP_740426.1, NP_740424.1) in FASTA format. The sequences were individually submitted to HHpred (Soding et al., 2005) for the identification of homologous protein structures for each subunit. As the study aimed to model the full TMEV GDVII protomer complex, only full protomer structures which contained template chains for all four protomer subunits were selected as possible templates. Initially, ten structures were selected as possible templates (supplementary table S1). The structural alignment program PROMALS3D (Pei et al., 2008) was then used to align the target sequences of each respective GDVII protomer subunit to ten structural sequences corresponding to the subunits of selected protomer templates. To ensure that the subunit-subunit interfaces were modelled correctly, each protomer template was submitted to the Protein Interactions Calculator (PIC) (Tina et al., 2007) for the identification of residues involved in inter-protein interactions. As each of the four subunits interacts with three other subunits, a total of 12 interfaces were examined. The interacting residues, predicted for each subunit-subunit interface, were then mapped to the respective multiple sequence alignments using in-house scripting. To assess the conservation of interface residues against the target sequences, the resulting alignments were visualised in Jalview (Waterhouse et al., 2009). An example of this analysis is shown for the VP1 subunit in supplementary Fig. S1. Subsequent to the observation that predicted interacting residues were highly conserved across the ten structures the final template selection was based on the following criteria: i) highest average sequence identity to the target protomer as calculated

across all four subunit proteins, ii) template resolution and iii) the sequence identity to the VP1 subunit (supplementary table S1). The crystal structures of TMEV DA (PDB ID: 1TME) and HEV-D68 (PDB ID: 4WM8) were selected as templates for the modelling of the TMEV GDVII protomer (supplementary table S2).

2.1.2 Model building and validation

Homology models of the full TMEV GDVII protomer complex were calculated using MODELLER 9v15 (Sali and Blundell, 1993), set to generate 100 unique models through very slow refinement. Given that the TMEV DA structure (PDB ID: 1TME) had high sequence identity to the target; an initial model set based only on this template was constructed. In an attempt to improve the quality of the models, a second model set based on a combination of TMEV DA with the higher resolution structure of HEV-D68 (PDB ID: 4WM8) was constructed. The models were initially evaluated according to the normalized DOPE-Z score (supplementary table S3). To validate the models' subunit interfaces the three best scoring models from each set were submitted to PIC followed by the mapping of predicted interacting residues to multiple sequence alignments. The models were also visualised in PyMOL (Schrodinger, 2010) for the identification of any geometric discrepancies. The top scoring model was additionally evaluated using PROSA (Wiederstein and Sippl, 2007).

2.2 Prediction of linear epitope regions on the surface of TMEV GDVII VP1

Linear epitope regions within TMEV GDVII VP1 were predicted using the webservers EliPro (Ponomarenko et al., 2008) and BepiPred (Larsen et al., 2006). The predicted VP1 epitopes were mapped to the homology model of the TMEV GDVII protomer to validate surface accessibility of these regions when the VP1 subunit is in an assembled protomer complex. The mapping and structural analysis was performed in PyMOL (Schrodinger, 2010). To investigate the epitope regions which were more likely to be soluble the GDVII VP1 sequence was submitted to Protscale (Gasteiger et al., 2005) for the prediction of hydrophobic and hydrophilic regions based on the Kyte and Doolittle method (Kyte and Doolittle, 1982).

2.3 Prediction of nuclear localisation signals and multiple sequence alignment of the C-terminus of VP1

The VP1 sequences of TMEV GDVII (NCBI: NP_740427), CVB3 (GenBank accession: U57056), EV71 (GenBank accession: HQ882182) and FMDV (GenBank accession: CAA00045) were retrieved from the GenBank database. The sequences were individually submitted to NucPred (Brameier et al., 2007) and SeqNLS (Lin and Hu, 2013) for the prediction of a nuclear localisation site. For identification of amino acid mutations the sequences were aligned using Promals3D (Pei et al., 2008) and visualised in Jalview (Waterhouse et al., 2009).

2.4 Plasmids

TMEV VP1 (1-112) was expressed in the *E. coli* strain JM109 from plasmid pCRTVP1. To create this plasmid, nucleotides 1-336 of the TMEV VP1 coding sequence were PCR-amplified from the TMEV GDVII cDNA, using the KAPA Taq ReadyMix kit (KAPA Biosystems, Cape Town, South Africa) and gene-specific oligonucleotide primers. The PCR product was ligated into plasmid pQE-80L (Qiagen, Mannheim, Germany) by restriction with *Bam*HI and *Sal*I. To confirm the presence of the insert and correct open reading frame, plasmid pCRTVP1 was sequenced by Inqaba Biotechnical Industries (Pty) Ltd., Pretoria South Africa.

2.5 Protein expression, SDS-PAGE and Western blotting

E. coli cells transformed with pCRTVP1 and pQE-80L were cultured in Luria broth (LB) supplemented with 100 µg/ml ampicillin at 37°C overnight. Cultures were induced with 1 mM Isopropyl β-D-1-thiogalactopyranoside (IPTG) for 4 hours and duplicate samples collected each hour. The cells were harvested by centrifugation at 11800 x *g* and pellets were resuspended to equivalent density in phosphate buffered saline [PBS; 137 mM NaCl, 2.7 mM KCl, 10 mM Na_2HPO_4, 2 mM KH_2PO_4 (pH 7.4)]. Proteins were denatured in 2X loading buffer and resolved by 12% SDS-PAGE before being transferred onto nitrocellulose membrane for Western blotting using Anti-His6 (2) antibodies. Detection was performed using the BM Chemiluminescence Western Blotting Kit (Roche, Mannheim, Germany) according to the manufacturer's instructions. Proteins were visualised using the ChemiDoc Molecular Imager XRS + (Bio-Rad, USA), and images were analysed using the Image Lab TM software, version 5.1.

2.6 Purification of VP1 (1-112)

An 80 ml overnight culture transformed with pCRTVP1 was induced and cells harvested by centrifugation at 6000 x *g*. Prior to sonication for 1 min on ice, the pellets were resuspended in ice cold 1xLEW buffer [50 mM Na_2PO_4, 300 mM NaCl, (pH 8.0)] supplemented with 30 mM imidazole and 7.5% N-Lauroylsarcosine (sarcosyl). Samples were clarified by centrifugation to obtain the supernatants which were pooled and purified using Protino Ni-IDA packed columns (Machery-Nagel). The peptide was eluted with 1xElution buffer [50 mM Na_2PO_4, 300 mM NaCl, 250 mM imidazole, (pH 8.0)]. The protein concentrations of eluted fractions were determined by Bradford's assay. Purified protein was concentrated in VIVASPIN 4 columns (Satorius Stedim Biotech, South Africa). A total of 1.2 mg purified TMEV VP1 (1-112) was used for rabbit immunisation.

2.7 Antibodies

Anti-His6 (2) (1:3000) recognising the 6x histidine tag on pQE80-L were purchased from Roche (Mannheim, Germany). Polyclonal antibodies against TMEV VP1 (1-112) were generated in rabbits by D. Bellstedt (University of Stellenbosch, South Africa). Rabbit antibodies against TMEV GDVII non-structural protein 2C were used at a concentration 1:1000 for indirect immunofluorescence (Jauka et al., 2010). Antibodies recognising Hsp90α and β isoforms (SC-13119) were from Santa Cruz Biotech, Santa Cruz, USA and used at 1:100.

2.8 Cells, viruses and infections

BHK-21 cells (kindly provided by M. Ryan, University of St Andrews, UK) were cultured in buffered Dulbecco's modified Eagle Medium (DMEM, Lonza Group Ltd, Basel, Switzerland) supplemented with 10% heat-inactivated foetal calf serum, 100 U penicillin ml^{-1}, 10 mg streptomycin ml^{-1} and 25 μg fungizone ml^{-1} at 37°C with 10% CO_2. TMEV strain GDVII was used to infect cells in all experiments. Virus stocks were prepared and titred using BHK-21 cells as described previously (Murray et al., 2009). For indirect immunofluorescence experiments, cells were infected at a multiplicity of infection (M.O.I) of approximately 3.

2.9 Preparation of infected cell lysate for Western blot

For the Western blot of infected lysates, cells were collected by centrifugation at 1000 x *g* and resuspended in 200 µl PBS. Total proteins were denatured and resolved by 12% SDS–PAGE before transfer onto nitrocellulose membrane for Western blotting using anti-TMEV VP1 antibodies. The BM Chemiluminescence Western Blotting kit (Roche, Mannheim, Germany) was used to detect viral protein according to manufacturers' instructions.

2.10 Indirect immunofluorescence and confocal microscopy

Cells grown on sterile 13 mm glass coverslips to 100% confluency in six-well plates containing complete medium were washed twice with serum-free DMEM before the addition of 1 ml of TMEV GDVII virus stock and 1 ml serum-free DMEM. Following incubation for 1 hour at 25˚C, cells were rinsed with PBS and 5 ml DMEM was added. The cells were incubated at 37º C, and lysates were prepared at 5 hours post infection (hpi). Control cells were mock-infected with serum-free DMEM. At 5 hpi, cells were collected by trypsinisation and washed with PBS before fixation with 4% paraformaldehyde for 20 min at room temperature (RT). For staining, cells were permeabilised in PB (10% sucrose, 1% Triton X-100 in PBS), blocked in PB containing 2% BSA for 30 min at RT and incubated with primary antibodies for 1 hour with shaking. Cells were washed with PBS containing 0.1% Tween-20, and incubated with species-specific Alexa Fluor 488-conjugated and/or Alexa Fluor 546-conjugated secondary antibodies for 30 min, followed by three washes. To stain the nucleus, 4',6-diamino-2-phenylindole dihydrochloride (DAPI, Sigma, St Louis, USA) was added at a concentration of 0.8 µg/ml in the second wash step. Cells were mounted using Dakofluorescence mounting medium (Dako Inc, CA, USA) and stored at RT. The helium/neon and argon lasers at wavelengths 405, 488 and 543 nm were used to excite DAPI, Alexa-fluor 488 and Alexa-fluor 546 respectively. Images were captured using the Zeiss LSM 510-Meta laser scanning confocal microscope and analysed using Zen software (blue edition, Zeiss, Germany). In order to acquire a representative image for each experiment, over 100 cells were viewed at 63 x magnification. Colocalisation analysis was performed on five randomly selected cells. Immunofluorescence experiments were performed in triplicate.

3. Results

3.1 Homology modelling of the TMEV GDVII protomer complex

The TMEV GDVII VP1 protein exists in complex with 3 other heterogenic subunits VP2-VP4. To distinguish predicted VP1 epitopes which remain exposed in the protomer complex from those which reside in an inter-subunit interface the 3D structure of the full TMEV GDVII protomer was calculated based on the known structures of homologous viral protomers (supplementary table S2). Initially ten crystal structures of homologous protomer structures were identified as possible templates (supplementary table S1). As explained in the Methodology section, out of ten two structures were chosen as final templates for model building (supplementary table S2). The structure 1TME was selected as a result of its high sequence identity to the GDVII protomer. The second structure 4WM8 was selected due to its higher resolution and was to be used in combination with 1TME in an attempt to improve model quality.

A primary aim of the study was to predict epitope regions within the VP1 subunit. Therefore, irrespective of the low sequence identity of 4WM8 to the full GDVII protomer, the template was still used as the VP1 subunits were 50% identical to each with the interface residues conserved. We constructed two different sets of models based on i) the lower resolution but high sequence identity template 1TME and ii) a combination of 1TME with a higher resolution template 4WM8. It must be noted that 1TME and 4WM8 were in the same conformation. The initial evaluation of the normalised DOPE-Z scores revealed a substantial increase in the quality of the models generated by a combination of 1TME and 4WM8 (supplementary table S3). For additional validation, the top three models of the GDVII protomer from each set were submitted to PIC for the prediction of interacting interface residues. The interacting residues were mapped to MSAs of the respective subunits of the six GDVII models. The MSAs also included the template sequences of 1TME and 4WM8. The interacting residues within all subunit-subunit interfaces predicted for both sets of GDVII models were completely conserved in the alignments. An example of this validation is shown in supplementary Fig. S2. The structural investigation of the models using PyMOL revealed no obvious geometric discrepancies. Since there was no improvement in the interface residues based on the use of the single but higher identity template 1TME, the best scoring model was selected based on the combination of 1TME and 4WM8 for epitope prediction.

The program PROSA was used to further investigate the overall quality of the selected model. As shown in supplementary Fig. S3, the z-scores of each subunit chain are comparable with all experimentally determined chains in the current PDB. PROSA was also used to investigate the local model quality, by plotting average residue energy scores over

each 40-residue fragment in each subunit (supplementary Fig. S4). The low occurrence of positive values indicates high model quality, with very few problematic regions.

3.2 Prediction of linear epitope regions on the surface of TMEV GDVII VP1

Linear B-cell epitope regions within TMEV GDVII VP1 were predicted using the webservers ElliPro and BepiPred. ElliPro incorporates the Thornton method (Thornton et al., 1986) for the prediction of epitopes on the surface of a protein structure. As shown in Fig. 2A, ElliPro identified major epitopes at both the N and C-termini of modelled GDVII VP1. Epitopes were also predicted in the central region of the protein ranging from residues 140-220. To substantiate these ElliPro results, the BepiPred method was applied. BepiPred is a sequence based method, and uses a combination of hidden Markov Models and propensity scales. The results (Fig. 2B) predict five epitopes in the N-terminal region with three major epitopes spanning the amino acids VP1 (1-18), VP1 (47-59) and VP1 (74-90). A comparative analysis of the ElliPro and BepiPred predictions indicated five overlapping epitope regions within the first 100 amino acids of the protein (supplementary table S4), while the predictions directly contradicted in the central residues 170-200.

Successful immunisation requires a substantial amount of soluble protein. Therefore, we aimed to express a VP1 region which was likely to be soluble as well as contain linear epitopes to elicit an immune response. A Kyte-Doolittle plot was used to assess the hydrophobicity across the GDVII VP1 protein. The results indicated a hydrophobic region spanning the residues 120-200, as opposed to several hydrophilic peaks located in the N-terminal region (supplementary Fig. S5). Subsequent to this observation it was hypothesised that the N-terminal region of VP1 had a higher likelihood of being soluble than the central region of the protein.

To structurally determine the surface accessibility of the overlapping epitopes in the N-terminal region ranging from the residues 1-105, the predicted epitopes were mapped into the GDVII protomer in PyMOL (Fig. 3). The structural mapping indicated that all five epitopes are surface exposed in the protomer complex. The protomers assemble to form pentamer structures and later a full capsid, where the protomer has an external and internal capsid face. The horizontal rotation of the protomer showed in Figs. 3A and 3B, revealed the location of 3 epitopes which reside externally and 2 epitopes on the internal face of the complex. Antibodies have been reported to also bind to the internal region of VP1 exposed during capsid breathing in Poliovirus 1 (Lin et al., 2012) and Parechovirus 1 (Kalynych et al., 2015). It was therefore hypothesised that generating polyclonal antibodies against a peptide

spanning the full VP1 (1-105) region, would result in antibodies which would recognise the VP1 protein and in the assembled capsid. After the consideration of primer design, the region VP1 (1-112) was selected for expression, purification and antibody production.

3.3 VP1 (1–112) is expressed as a soluble peptide in the presence of sarcosyl

JM109 *E. coli* cultures harbouring pCRTVP1 and pQE-80L were grown to mid-log phase and induced with 1mM IPTG for 4 hours, in order to analyse the expression of VP1 (1-112). An over expressed peptide of approximately 19 kDa was detectable at 1 hour post-induction, and increased in intensity with time reaching a maximum at around 3 hours (Fig. 4A). The peptide was not evident at the start of the induction or in lysate from cells harbouring the empty pQE-80L vector (Fig. 4A). Western blot using anti-His_6 antibodies confirmed that the peptide was recombinant VP1 (1-112) (Fig. 4B).

To produce enough recombinant VP1 (1-112) for immunisation purposes, an 80ml culture of transformed *E.coli* JM109 cells, harbouring pCRTVP1 was induced with IPTG for 4 hours, divided into 2x40ml and cells were harvested through centrifugation. The cells were resuspended in 1XLEW [50 mM Na_2PO_4, 300 mM NaCl, (pH 8.0)] buffer supplemented with 30 mM imidazole and sonicated either in the absence or in the presence of 7.5% sarcosyl (data not shown). In the absence of sarcosyl, a significant amount of the peptide was found in the pellet. The addition of 7.5% sarcosyl increased the solubility of the peptide, with only small traces in the pellet and the majority of the peptide present in the soluble fraction (data not shown).

3.4 Anti-TMEV VP1 (1-112) antibodies recognise full length VP1 in infected cell lysates

To determine whether the resultant polyclonal anti-VP1 (1-112) antibodies could detect virally expressed VP1, BHK-21 cells were infected or mock-infected with TMEV for a period of 5, 8 and 24 hours. Total cell lysates were then analysed together with bacterially expressed VP1 (1-112) lysate by Western blot. A peptide of approximately 19 kDA representing VP1 (1-112) was detected in the bacterial lysate as expected (Fig. 5). The anti-TMEV VP1 (1-112) antibodies successfully detected a virally expressed protein of approximately 37 kDa in TMEV infected cell lysates and signal increased in intensity with time post infection (Fig. 5). No protein bands were detected in mock-infected cell lysate, indicating that the signal detected in infected lysates was a result of TMEV infection. Pre-

immune serum was not able to detect the 19 kDa or 37 kDa bands in bacterial or infected cell lysates (data not shown).

3.5 TMEV VP1 distributes in the cytoplasm and perinuclear region but not in the nucleus of infected cells

To examine the distribution of VP1 in TMEV-infected cells, BHK-21 cells were infected or mock-infected with TMEV, fixed with paraformaldehyde at 5 hpi, and immunostained with anti-TMEV VP1 and 2C antibodies. No signal was observed in either mock-infected cells (Fig. 6A panel a) or in infected cells stained with secondary antibodies alone (Fig. 6A panel b). To confirm that cells were TMEV infected and to compare VP1 distribution, previously generated anti-TMEV 2C antibodies (Jauka et al., 2010) were used (Fig. 6A panel c). The 2C signal appears dominant in the perinuclear region as previously reported (Jauka et al., 2010; Mutsvunguma et al., 2011). Following the optimisation of anti-TMEV VP1 (1-112) antibodies using different dilutions (data not shown), the VP1 signal was diffusely cytoplasmic and in the perinuclear region but absent from the nucleus of infected cells at 5 hpi (Fig. 6A panel d). Importantly, all infected cells observed at this time point in three separate experiments showed the same cytoplasmic distribution pattern for VP1. Following analysis of the TMEV VP1 sequence, no typical NLS was observed. Likewise, the programs used did not detect a NLS in the VP1 sequences of CVB3, EV71 or FMDV. A multiple alignment of C-terminal VP1 regions of TMEV, FMDV, EV71 and CVB3 shown in Fig. 6B showed that the basic histidine residue at position 220, suggested to be responsible for nuclear localisation of CBV3, was replaced by threonine in EV71 VP1, glycine in TMEV VP1 and valine in FMDV.

3.6 TMEV VP1 colocalises with Hsp90 at 5 hours post infection

To examine the sub-cellular distribution of VP1 in relation to Hsp90 during infection, cells grown on coverslips were infected with TMEV, fixed with paraformaldehyde at 5 hpi and co-stained with Hsp90 and anti-TMEV VP1 (1-112) antibodies. No signal for VP1 was observed in mock-infected cells probed with anti-TMEV VP1 antibodies (Fig. 7A). The distribution of Hsp90 in mock-infected cells was diffuse and cytoplasmic (Fig. 7A panel a) but changed at 5 hpi becoming more intense in the perinuclear region (Fig. 7B panel d). Interestingly, the signals for TMEV VP1 and Hsp90 colocalised extensively in the cytoplasm and perinuclear region (displayed by white pixels in Fig. 7B panel f). Moreover, the frequency scatter plots indicate a high degree of colocalisation between the two signals (Fig. 7B panel g). The profile

taken along a section of the TMEV infected cell (Fig. 7 panel h) shows that the green (VP1) and red (Hsp90) signal intensities correlate with each other throughout the cell with increased intensity in the perinuclear region compared to the cytoplasm. In comparison, Hsp90 and 2C signal was largely perinuclear and colocalised in this region (Fig. 7C panels i-k). The frequency scatterplot confirmed colocalisation (Fig. 7C panel l) and the profile clearly shows that red (Hsp90) and green (2C) signal intensities were less correlated in the cytoplasm than in the case of VP1, and increased asymmetrically in the perinuclear region (Fig. 7 panel m). The above analysis was performed on five randomly selected cells co-stained with anti-VP1/anti-2C and Hsp90 antibodies.

4. Discussion

The primary aim of this study was to generate antibodies against the TMEV GDVII VP1 protein subunit and test their specificity in detecting VP1 in infected cells by Western blotting and indirect immunofluorescence. To date, very few studies describe the localisation of picornavirus capsid subunits in cells at early stages of virus assembly which remains a poorly understood process in the virus life cycle. There is substantial evidence to suggest that picornavirus replication and assembly take place on the surface of specialised membrane vesicles and that the viral proteins associate with these membranes (Bienz et al., 1983; Egger et al., 2002; Jackson et al., 2005; Schwartz et al., 2004) thereby complicating their solubilisation and purification in a heterologous system for downstream applications. Indeed, previous attempts to solubilise and purify the full-length TMEV VP1 protein were unsuccessful. To address this problem, a bioinformatics approach was used to map a region on VP1 predicted to contain surface-exposed linear B-cell epitopes, and which could be purified in a soluble form for immunisation purposes. Because VP1 exists as part of a protomer complex within the viral capsid, homology modelling was used to generate a 3D structure of the TMEV protomer complex to accurately predict and assess the surface accessibility of linear epitopes on the protein. Furthermore, since VP1 is an antigenic determinant of the capsid, it was reasonable to assume that antibodies generated against an immunogenic VP1 peptide would also recognise the full-length protein as well as viral capsids in infected cells. Following a bioinformatics analysis of VP1, the N-terminal region (amino acids 1-112) was predicted to contain surface linear B-cell epitopes at amino acid positions 1-18, 24-30, 50-56, 78-88, 98-105, and was selected for bacterial expression and

purification. The antibodies were able to detect the bacterially expressed VP1 peptide (1-112) as expected, but were also specific in detecting full length VP1 protein in TMEV-infected cells lysates with no contaminating proteins. Because lysates were not fractionated in these experiments, it cannot be concluded that TMEV VP1 is present predominantly in a membrane-associated or soluble form. It is surprising that the P1 precursor protein was not detected in infected cell lysates using anti-TMEV VP1 antibodies. This observation will be further investigated and if found to be valid, indicates that these antibodies are an extremely useful tool in investigating the localisation and interactions of VP1 with host components during virus assembly.

To investigate the localisation of VP1 in TMEV-infected BHK-21 cells, the next experiments examined the specificity of the anti-TMEV VP1 (1-112) antibodies in detecting VP1 in cells by indirect immunofluorescence and confocal microscopy at 5 hpi. A clear signal was detected in infected cells but not in mock infected cells indicating that the antibodies were specific for VP1 at an optimal dilution of 1:20 000. The distribution of TMEV VP1 at 5 hpi was diffusely cytoplasmic with increased signal intensity in the perinuclear region. This pattern was observed in over 100 cells (data not shown). Cytoplasmic VP1 may represent soluble protein at this stage of infection and preliminary experiments using anti-VP1 antibodies indicate that VP1 is present in both membrane and supernatant fractions (data not shown). Interestingly, TMEV VP1 was not observed in the nucleus at 5 hpi. The capsid proteins of several RNA viruses such as West Nile Virus (WNV) (Bhuvanakantham et al., 2010), porcine reproductive and respiratory syndrome virus (PRRSV) (Pei et al., 2009), Dengue virus (Colpitts et al., 2011) and the picornavirus CVB3 (Wang et al., 2012), have been reported to translocate to the nucleus during infection where they interfere with essential nuclear functions. Proteins targeted to the nucleus in cells typically possess a C-terminal nuclear localisation signal (NLS) consisting of a stretch of basic amino acids that is bound by nuclear import receptors (McLane and Corbett, 2009). For the identification of possible NLS's, the full length VP1 sequences of TMEV, FMDV, CVB3 and EV71 were analysed *in silico* by NucPred and SeqNLS. Both programs indicated the absence of a typical NLS in all four viral proteins. However, previous analysis of the CVB3 VP1 sequence showed that, although the protein did not display a typical NLS, a C-terminal histidine residue at position 220 (H220) was a critical determinant required for active translocation to the nucleus (Wang et al., 2012). To investigate whether this residue is present in TMEV and other related viruses, a multiple sequence alignment between VP1 C-terminal sequences of several

picornaviruses was performed. The H220 in CVB3 was substituted for threonine in EV71 VP1 which has been shown to distribute in the cytoplasm of infected cells (Liu et al., 2013; Wang et al., 2012). The lack of a typical NLS and observation that H220 is replaced by glycine in TMEV VP1 provides an explanation for the similar cytoplasmic distributions of EV71 and TMEV VP1 proteins. Similarly in FMDV VP1, the H220 residue is replaced by valine. Interestingly, the distribution of TMEV VP1 at 5 hpi was not unlike that of FMDV during late infection where VP1 localised predominantly to the perinuclear region of FMDV infected cells and colocalised with the replication protein 2C (Knox et al., 2005).

Hsp90 has vital functions in the cell including protein folding and trafficking, maintenance of protein stability and regulation of cell growth and differentiation (Passinen et al., 2001; Picard, 2004; Pratt and Toft, 2013; Zhang et al., 2013). Hsp90 is upregulated under conditions of stress, including viral infection, and is required for the replication and capsid assembly of many viruses, including picornaviruses such as PV and HRV (Geller et al., 2012). Therefore the next experiments investigated the localisation of VP1 relative to Hsp90 during TMEV infection. In 5-hour infected cells, the Hsp90 signal was greater in intensity compared to mock-infected cells and became concentrated in the perinuclear region where it colocalised with VP1. The staining pattern for Hsp90 at 5 hpi observed in this study concurs with that reported by Mutsvunguma et al. (2011) where the distribution of Hsp90 was time dependent, moving from a diffuse cytoplasmic staining pattern during early infection and becoming concentrated in the perinuclear region at later time points.

Interestingly, VP1 and Hsp90 showed good signal correlation in infected cells where colocalisation occurred in the cytoplasm and perinuclear region of infected cells. In comparison, Hsp90 and 2C signals were less correlated and colocalisation was only apparent in the juxtanuclear region. A five hour time point may be considered relatively early during TMEV infection as cytopathic effect is only observed from about 7 hpi. The data showing that Hsp90 and VP1 colocalise suggest that Hsp90 is required during the early stages of TMEV capsid assembly. These results support existing evidence that Hsp90 is involved in the picornavirus capsid assembly but may not be directly involved with virus replication (Geller et al., 2007).

In conclusion, this is the first study to report the distribution of TMEV VP1 in infected cells by Western blot and indirect immunofluorescence. Significantly, VP1 signal distribution was found to be cytoplasmic with greater signal intensity in the perinuclear region. This coupled

with its absence from the nucleus and the lack of a typical NLS indicate that TMEV VP1 behaves in a similar manner to that of picornaviruses such as FMDV and Enterovirus 71. Overlap between VP1 and Hsp90 distribution supports the previous observation that Hsp90 plays an important role for this chaperone in the TMEV life cycle (Mutsvunguma et al., 2011). The generation of TMEV VP1 specific polyclonal antibodies and their optimisation by Western blot and indirect immunofluorescence is an important milestone that has provided the tool and methodologies necessary for future studies investigating interactions between this capsid subunit and host cell factors to better understand not only the process of capsid assembly but also the mechanisms involved in the early stages of picornavirus entry.

Acknowledgements

The authors gratefully acknowledge H. Lipton for providing TMEV GDVII cDNA, and D. Lang for assistance with the confocal analysis. This work was supported by SIR (Medical Research Council, South Africa) and Research Council (RC, Rhodes University) grants. CR and ÖTB thank the National Research Foundation of South Africa (grant number 93690). NU was supported by postgraduate fellowships from the NRF and the German Academic Exchange Service (DAAD) and a Henderson Fellowship from Rhodes University. The content of this publication is solely the responsibility of the authors and does not necessarily represent official views of the funders.

References

Bedard, K.M., Semler, B.L., 2004. Regulation of picornavirus gene expression. Microbes Infect. 6, 702–713. doi:10.1016/j.micinf.2004.03.001

Bhuvanakantham, R., Cheong, Y.K., Ng, M.L., 2010. West Nile virus capsid protein interaction with importin and HDM2 protein is regulated by protein kinase C-mediated phosphorylation. Microbes Infect. 12, 615–625. doi:10.1016/j.micinf.2010.04.005

Bienz, K., Egger, D., Rasser, Y., Bossart, W., 1983. Intracellular distribution of poliovirus proteins and the induction of virus-specific cytoplasmic structures. Virology 131, 39–48.

Bobek, V., Kolostova, K., Pinterova, D., Kacprzak, G., Adamiak, J., Kolodziej, J., Boubelik, M., Kubecova, M., Hoffman, R.M., 2010. A clinically relevant, syngeneic model of

spontaneous, highly metastatic B16 mouse melanoma. Anticancer Res. 30, 4799–4804. doi:10.1002/jmv

Brameier, M., Krings, A., MacCallum, R.M., 2007. NucPred - Predicting nuclear localization of proteins. Bioinformatics 23, 1159–1160. doi:10.1093/bioinformatics/btm066

Brito, B.P., Rodriguez, L.L., Hammond, J.M., Pinto, J., Perez, A.M., 2015. Review of the Global Distribution of Foot-and-Mouth Disease Virus from 2007 to 2014. Transbound. Emerg. Dis. n/a–n/a. doi:10.1111/tbed.12373

Cameron, K., Zhang, X., Seal, B., Rodriguez, M., Njenga, M.K., 2001. Antigens to viral capsid and non-capsid proteins are present in brain tissues and antibodies in sera of Theiler's virus-infected mice. J. Virol. Methods 91, 11–19. doi:10.1016/S0166-0934(00)00246-9

Collen, T., Dimarchi, R., Doel, T.R., 1991. A T cell epitope in VP1 of foot-and-mouth disease virus is immunodominant for vaccinated cattle. J. Immunol. 146, 749–755.

Colpitts, T.M., Barthel, S., Wang, P., Fikrig, E., 2011. Dengue virus capsid protein binds core histones and inhibits nucleosome formation in human liver cells. PLoS One 6. doi:10.1371/journal.pone.0024365

Edlmayr, J., Niespodziana, K., Popow-Kraupp, T., Krzyzanek, V., Focke-Tejkl, M., Blaas, D., Grote, M., Valenta, R., 2011. Antibodies induced with recombinant VP1 from human rhinovirus exhibit cross-neutralisation. Eur. Respir. J. 37, 44–52. doi:10.1183/09031936.00149109

Egger, D., Wölk, B., Gosert, R., Bianchi, L., Blum, H.E., Moradpour, D., Bienz, K., 2002. Expression of hepatitis C virus proteins induces distinct membrane alterations including a candidate viral replication complex. J. Virol. 76, 5974–84. doi:10.1128/JVI.76.12.5974

Gasteiger, E., Hoogland, C., Gattiker, A., Duvaud, S., Wilkins, M.R., Appel, R.D., Bairoch, A., 2005. Protein Identification and Analysis Tools on the ExPASy Server, in: Walker, J.M. (Ed.), The Proteomics Protocols Handbook. Humana Press, pp. 571–607.

Geller, R., Taguwa, S., Frydman, J., 2012. Broad action of Hsp90 as a host chaperone required for viral replication. Biochim. Biophys. Acta - Mol. Cell Res. 1823, 698–706. doi:10.1016/j.bbamcr.2011.11.007

Geller, R., Vignuzzi, M., Andino, R., Frydman, J., 2007. Evolutionary constraints on chaperone-mediated folding provide an antiviral approach refractory to development of

drug resistance. Genes Dev. 21, 195–205. doi:10.1101/gad.1505307

Grant, R.A., Filman, D.J., Fujinami, R.S., Icenogle, J.P., Hogle, J.M., 1992. Three-dimensional structure of Theiler virus. Proc. Natl. Acad. Sci. U. S. A. 89, 2061–2065. doi:10.1073/pnas.89.6.2061

Hagan, J.E., Wassilak, S.G.F., Craig, A.S., Tangermann, R.H., Diop, O.M., Burns, C.C., 2015. Progress Toward Polio Eradication — Worldwide , 2014 – 2015. MMWR. Morb. Mortal. Wkly. Rep. 64, 2014–2015.

Jackson, W.T., Giddings, T.H., Taylor, M.P., Mulinyawe, S., Rabinovitch, M., Kopito, R.R., Kirkegaard, K., 2005. Subversion of cellular autophagosomal machinery by RNA viruses. PLoS Biol. 3, 0861–0871. doi:10.1371/journal.pbio.0030156

Jauka, T., Mutsvunguma, L., Boshoff, A., Edkins, A.L., Knox, C., 2010. Localisation of Theiler's murine encephalomyelitis virus protein 2C to the Golgi apparatus using antibodies generated against a peptide region. J. Virol. Methods 168, 162–169. doi:10.1016/j.jviromet.2010.05.009

Jiang, P., Liu, Y., Ma, H.-C., Paul, a. V., Wimmer, E., 2014. Picornavirus Morphogenesis. Microbiol. Mol. Biol. Rev. 78, 418–437. doi:10.1128/MMBR.00012-14

Kalynych, S., Palkova, L., Plevka, P., 2015. The structure of Human Parechovirus-1 reveals an association of the RNA genome with the capsid. J. Virol. doi:10.1128/JVI.02346-15

Knox, C., Moffat, K., Ali, S., Ryan, M., Wileman, T., 2005. Foot-and-mouth disease virus replication sites form next to the nucleus and close to the Golgi apparatus, but exclude marker proteins associated with host membrane compartments. J. Gen. Virol. 86, 687–696. doi:10.1099/vir.0.80208-0

Kyte, J., Doolittle, R.F., 1982. A simple method for displaying the hydropathic character of a protein. J. Mol. Biol. 157, 105–132. doi:10.1016/0022-2836(82)90515-0

Larsen, J.E.P., Lund, O., Nielsen, M., 2006. Improved method for predicting linear B-cell epitopes. Immunome Res. 2, 2. doi:10.1186/1745-7580-2-2

Li, C., Wang, J.C.Y., Taylor, M.W., Zlotnick, A., 2012. In Vitro Assembly of an Empty Picornavirus Capsid follows a Dodecahedral Path. J. Virol. 86, 13062–13069. doi:10.1128/JVI.01033-12

Lin, J., Hu, J., 2013. SeqNLS: nuclear localization signal prediction based on frequent pattern mining and linear motif scoring. PLoS One 8, e76864.

doi:10.1371/journal.pone.0076864

Lin, J., Lee, L.Y., Roivainen, M., Filman, D.J., Hogle, J.M., Belnap, D.M., 2012. Structure of the Fab-Labeled "Breathing" State of Native Poliovirus. J. Virol. 86, 5959–5962. doi:10.1128/JVI.05990-11

Lipton, H.L., 1975. Theiler ' s virus infection in mice : an unusual biphasic disease process leading to Theiler ' s Virus Infection in Mice : an Unusual Biphasic Disease Process Leading to Demyelination 11, 1147–1155.

Liu, Q., Huang, X., Ku, Z., Wang, T., Liu, F., Cai, Y., Li, D., Leng, Q., Huang, Z., 2013. Characterization of enterovirus 71 capsids using subunit protein-specific polyclonal antibodies. J. Virol. Methods 187, 127–131. doi:10.1016/j.jviromet.2012.09.024

Liu, Y., Sheng, J., Fokine, A., Meng, G., Shin, W.-H., Long, F., Kuhn, R.J., Kihara, D., Rossmann, M.G., 2015. Structure and inhibition of EV-D68, a virus that causes respiratory illness in children. Science 347, 71–4. doi:10.1126/science.1261962

Luo, M., He, C., Toth, K.S., Zhang, C.X., Lipton, H.L., 1992. Three-dimensional structure of Theiler murine encephalomyelitis virus (BeAn strain). Proc Natl Acad Sci U.S.A 89, 2409–2413.

Macejak, D.G., Sarnow, P., 1992. Association of heat shock protein 70 with enterovirus capsid precursor P1 in infected human cells. J. Virol. 66, 1520–1527.

Mansour, S.M.G., Ali, H., Chase, C.C.L., Cepica, A., 2015. Loop-mediated isothermal amplification for diagnosis of 18 World Organization for Animal Health (OIE) notifiable viral diseases of ruminants, swine and poultry. Anim. Heal. Res. Rev. 1–18. doi:10.1017/S1466252315000018

Mateu, M.G., 1995. Antibody recognition of picornaviruses and escape from neutralization: A structural view. Virus Res. 38, 1–24. doi:10.1016/0168-1702(95)00048-U

McLane, L.M., Corbett, A.H., 2009. Nuclear localization signals and human disease. IUBMB Life 61, 697–706. doi:10.1002/iub.194

Meloen Briaire, R.H.J., Woortmeyer, R.J., Van Zaane, D., 1983. The main antigenic determinant detected by neutralizing monoclonal antibodies on the intact foot-and-mouth disease virus particle is absent from isolated VP1. J. Gen. Virol. 64, 1193–1198.

Murray, L., Luke, G.A., Ryan, M.D., Wileman, T., Knox, C., 2009. Amino acid substitutions within the 2C coding sequence of Theiler's Murine Encephalomyelitis virus alter virus

growth and affect protein distribution. Virus Res. 144, 74–82. doi:10.1016/j.virusres.2009.04.001

Mutsvunguma, L.Z., Moetlhoa, B., Edkins, A.L., Luke, G.A., Blatch, G.L., Knox, C., 2011. Theiler's murine encephalomyelitis virus infection induces a redistribution of heat shock proteins 70 and 90 in BHK-21 cells, and is inhibited by novobiocin and geldanamycin. Cell Stress Chaperones 16, 505–515. doi:10.1007/s12192-011-0262-x

Oberste, M.S., Maher, K., Kilpatrick, D.R., Pallansch, M.A., 1999. Molecular evolution of the human enteroviruses: correlation of serotype with VP1 sequence and application to picornavirus classification. J. Virol. 73, 1941–8.

Oleszak, E.L., Chang, J.R., Friedman, H., Katsetos, C.D., Platsoucas, C.D., 2004. Theiler ' s Virus Infection : a Model for Multiple Sclerosis. Society 17, 174–207. doi:10.1128/CMR.17.1.174

Passinen, S., Valkila, J., Manninen, T., Syvälä, H., Ylikomi, T., 2001. The C-terminal half of Hsp90 is responsible for its cytoplasmic localization. Eur. J. Biochem. 268, 5337–5342. doi:10.1046/j.0014-2956.2001.02467.x

Pei, J., Kim, B.H., Grishin, N. V., 2008. PROMALS3D: A tool for multiple protein sequence and structure alignments. Nucleic Acids Res. 36, 2295–2300. doi:10.1093/nar/gkn072

Pei, Y., Hodgins, D.C., Wu, J., Welch, S.-K.W., Calvert, J.G., Li, G., Du, Y., Song, C., Yoo, D., 2009. Porcine reproductive and respiratory syndrome virus as a vector: immunogenicity of green fluorescent protein and porcine circovirus type 2 capsid expressed from dedicated subgenomic RNAs. Virology 389, 91–9. doi:10.1016/j.virol.2009.03.036

Picard, D., 2004. Hsp90 invades the outside. Nat. Cell Biol. 6, 479–480. doi:10.1038/ncb0604-479

Pratt, W.B., Toft, D.O., 2003. Regulation of signaling protein function and trafficking by the hsp90/hsp70-based chaperone machinery. Exp Biol Med 228, 111–133.

Ponomarenko, J., Bui, H.H., Li, W., Fusseder, N., Bourne, P.E., Sette, A., Peters, B., 2008. ElliPro: a new structure-based tool for the prediction of antibody epitopes. BMC Bioinformatics 9, 514. doi:10.1186/1471-2105-9-514

Rombaut, B., Foriers, A., Boeye, A., 1991. In vitro assembly of poliovirus 14 S subunits: Identification of the assembly promoting activity of infected cell extracts. Virology 180,

781–787. doi:10.1016/0042-6822(91)90091-O

Rossmann, M.G., Arnold, E., Erickson, J.W., Frankenberger, E.A., Griffith, J.P., Hecht, H.J., Johnson, J.E., Kamer, G., Luo, M., Mosser, A.G., 1985. Structure of a human common cold virus and functional relationship to other picornaviruses. Nature 317, 145–153. doi:10.1038/317145a0

Rotbart, H.A., Hayden, F.G., 2000. Picornavirus infections: a primer for the practitioner. Arch. Fam. Med. 9, 913–920. doi:10.1001/archfami.9.9.913

Rueckert, R.R., 1996. Picornaviridae: the viruses and their replication, in: Fields, B.N., Knipe, D.M., Howley, P.M., Chanock, R.M., Melnick, J.L., Monath, T.P., Roizman, B., Straus, S.E. (Eds.), Virology, 3rd ed. Raven Press, Ltd., New York, N.Y., pp. 609-654.

Sali, A., Blundell, T.L., 1993. Comparative Protein Modelling by Satisfaction of Spatial Restraints. J. Mol. Biol.

Schrodinger, L.L.C., 2010. The PyMOL Molecular Graphics System, Version 1.3r1.

Schwartz, M., Chen, J., Lee, W.M., Janda, M., Ahlquist, P., 2004. Alternate, virus-induced membrane rearrangements support positive-strand RNA virus genome replication. Proc. Natl. Acad. Sci. U. S. A. 101, 11263–11268. doi:10.1073/pnas.0404157101

Soding, J., Biegert, A., Lupas, A.N., 2005. The HHpred interactive server for protein homology detection and structure prediction. Nucleic Acids Res. 33, W244–W248. doi:10.1093/nar/gki408

Tan, C.S., Cardosa, M.J., 2007. High-titred neutralizing antibodies to human enterovirus 71 preferentially bind to the N-terminal portion of the capsid protein VP1. Arch. Virol. 152, 1069–73. doi:10.1007/s00705-007-0941-1

Thornton, J.M., Edwards, M.S., Taylor, W.R., Barlow, D.J., 1986. Location of "continuous" antigenic determinants in the protruding regions of proteins. EMBO J. 5, 409–413.

Tina, K.G., Bhadra, R., Srinivasan, N., 2007. PIC: Protein Interactions Calculator. Nucleic Acids Res. 35, 473–476. doi:10.1093/nar/gkm423

Varrasso, A., Drummer, H.E., Huang, J.A., Stevenson, R.A., Ficorilli, N., Studdert, M.J., Hartley, C.A., 2001. Sequence conservation and antigenic variation of the structural proteins of equine rhinitis A virus. J. Virol. 75, 10550–10556. doi:10.1128/jvi.75.21.10550-10556.2001

Wang, T., Yu, B., Lin, L., Zhai, X., Han, Y., Qin, Y., Guo, Z., Wu, S., Zhong, X., Wang, Y., Tong, L., Zhang, F., Si, X., Zhao, W., Zhong, Z., 2012. A functional nuclear localization sequence in the VP1 capsid protein of coxsackievirus B3. Virology 433, 513–521. doi:10.1016/j.virol.2012.08.040

Waterhouse, A.M., Procter, J.B., Martin, D.M.A., Clamp, M., Barton, G.J., 2009. Jalview Version 2-A multiple sequence alignment editor and analysis workbench. Bioinformatics 25, 1189–1191. doi:10.1093/bioinformatics/btp033

Wiederstein, M., Sippl, M.J., 2007. ProSA-web: interactive web service for the recognition of errors in three-dimensional structures of proteins. Nucleic Acids Res. 35, W407–W410. doi:10.1093/nar/gkm290

Wu, C.N., Lin, Y.C., Fann, C., Liao, N.S., Shih, S.R., Ho, M.S., 2001. Protection against lethal enterovirus 71 infection in newborn mice by passive immunization with subunit VP1 vaccines and inactivated virus. Vaccine 20, 895–904. doi:10.1016/S0264-410X(01)00385-1

Zhang, J., Li, J., Liu, B., Zhang, L., Chen, J., Lu, M., 2013. Genome-wide analysis of the Populus Hsp90 gene family reveals differential expression patterns, localization, and heat stress responses. BMC Genomics 14, 532. doi:10.1186/1471-2164-14-532

Figure Captions

Fig 1. Assembly of Picornavirus particles. Hsp90 mediates a conformational change in the P1 precursor, allowing cleavage by the 3CD and 3C proteases. Resulting VP0, VP1 and VP3 capsid proteins form the capsomer, of which 5 combine to produce the pentamer. 12 pentamers then associate around the mRNA genome to generate the provirion. VP0 is then cleaved yielding the outer facing VP2 capsid protein and the internally oriented VP4 protein, maturing the newly formed virion. Alternatively 12 pentamers can assemble without inclusion of the mRNA genome to yield empty 80S procapsids. Purified pentamers are able to assemble into empty procapsids in a cell free test tube environment through “self-assembly”, indicating that assembly from pentamer to capsid maturation is based on protein-protein interactions (Li et al., 2012). However the stages from P1 precursor cleavage to

pentamer formation remain enigmatic, and seem to require both viral and host cell factors. Adapted from Jiang et al. (2014).

Fig 2. Predicted linear B-cell epitopes within TMEV GDVII VP1 protein. A) An ElliPro plot of predicted linear B-cell epitopes based on the homology model of the GDVII protomer. B) BepiPred plot of predicted linear B-cell epitope regions based on the primary amino acid sequence of GDVII VP1. Predicted epitopes are indicated by positive peaks. The peptide region selected for antigen production is indicated by the black dashed arrow: VP1 (1-112).

Fig 3. Homology model of the TMEV GDVII protomer complex showing predicted VP1 linear B-cell epitopes. The model based on two homologous viral protomer structures of Theiler's Virus (1TME) and Enterovirus D68 (4WM8), was generated using MODELLER. The model has been coloured by subunit: green - VP1; cyan - VP2; pink - VP3; yellow - VP4; orange - amino acid regions predicted to map to linear B-cell epitopes as predicted by both ElliPro and BepiPred. A) PyMOL generated image showing epitope regions VP1: 50-56; 78-88; 98-105. B) Horizontal rotation of the 3D structure showing epitope regions VP1: 1-18 and 24-30.

Fig 4. Expression and analysis of TMEV VP1 (1-112) protein. (A) SDS-PAGE analysis of an induction study of VP1 (1-112) over time. The protein represents total cell extract over time after induction with 1 mM IPTG. MW (molecular weight marker in kDa). Cells were transformed with pCRTVP1 and induced hourly for 4 hours using IPTG. Cells were transformed with pQE80-L and induced for 4 hours using IPTG (negative control). (B) Expression of His-tagged TMEV VP1 (1-112) confirmed by Western blot using anti-His6 antibodies.

Fig 5. Detection of recombinant VP1 (1-112) and full-length VP1. Western blot of bacterially expressed lysate and TMEV infected BHK-21 lysates at various times post-infection, using anti-TMEV VP1 (1-112) peptide antibodies. MW (molecular weight marker in kDa).

Fig 6. A) Distribution of TMEV VP1 in 5-hour infected BHK-21 cells. Cells were mock infected (panel a) or infected with TMEV (panels b, c and d), fixed with paraformaldehyde at 5 hpi and stained with anti-TMEV VP1 (1-112) (panels a and d), or anti-TMEV 2C (panel c) antibodies. Primary antibodies were detected with species-specific Alexa Fluor 488-conjugated secondary antibodies. Cells in panel b were stained with Alexa Fluor 488-

conjugated secondary antibodies only. Scale bars = 20 μm. **B) Multiple sequence alignment of the C-terminus of VP1 proteins of CVB3, EV71, TMEV and FMDV.** Full length protein sequences were retrieved from GenBank and aligned using Promals3D. The aligned C-terminus region was subsequently visualised in Jalview. The arrow indicates the site of substitution from basic histidine in CVB3 to the neutral residues threonine, glycine and valine in EV71, TMEV and FMDV respectively.

Fig 7. Distribution of TMEV VP1 and 2C in relation to Hsp90. Cells were either mock infected (A) or infected with TMEV (B and C), paraformaldehyde fixed at 5 hpi, and co-stained with antibodies against TMEV VP1 (A and B) or 2C (C), as well as antibodies against Hsp90 α/β. Primary antibodies were detected with species-specific Alexa-Fluor 488 or Alexa-Fluor 546-conjugated secondary antibodies respectively. Scale bars = 20 μm. Merged Hsp90 and TMEV signals are displayed in the form of colocalisation maps (panels c, f and k), where colocalised pixels are shown in white. Signal intensity profiles for green, red, and blue (DAPI) channels along a section of the TMEV infected cells are depicted in panels h and m. Frequency scatter plots of the intensity registered in the red and green channels of infected cells indicate the degree of colocalisation between signals for Hsp90 and TMEV (panels g and l). Hsp90 signal is always shown on the x axis, whereas the y axis corresponds to the intensity of the TMEV signal.

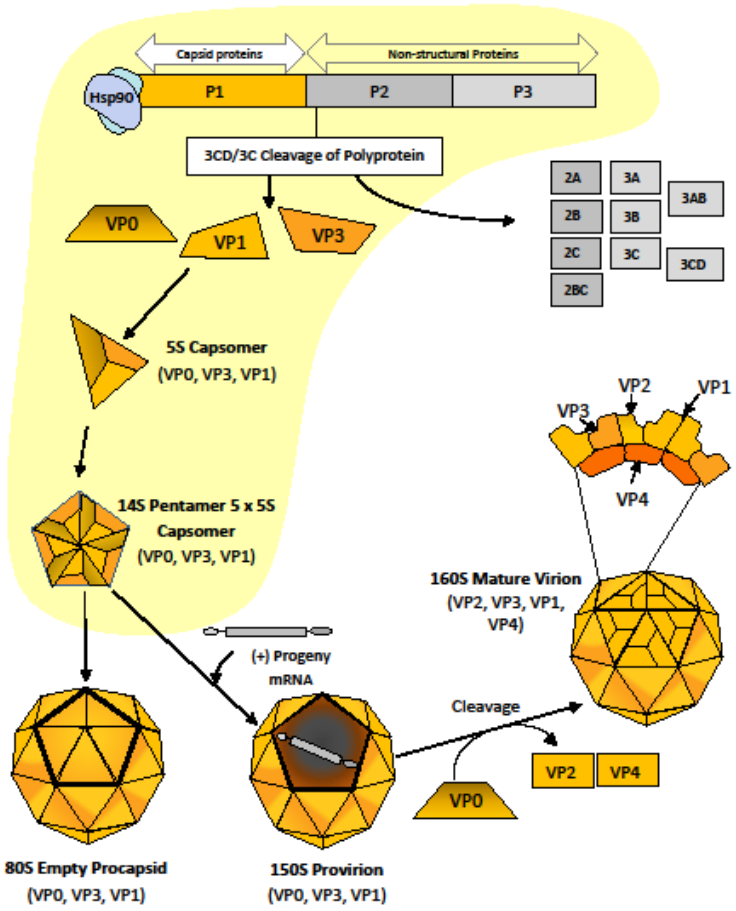

Fig. 1

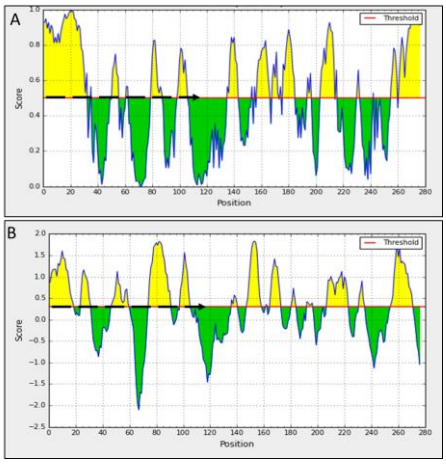

Fig. 2

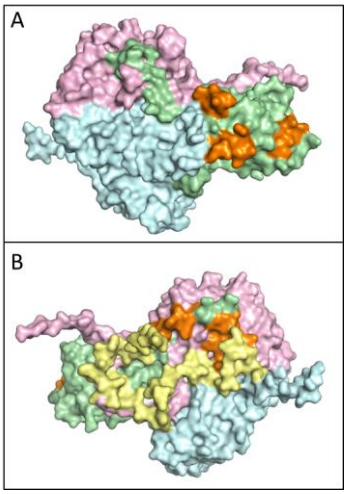

Fig. 3

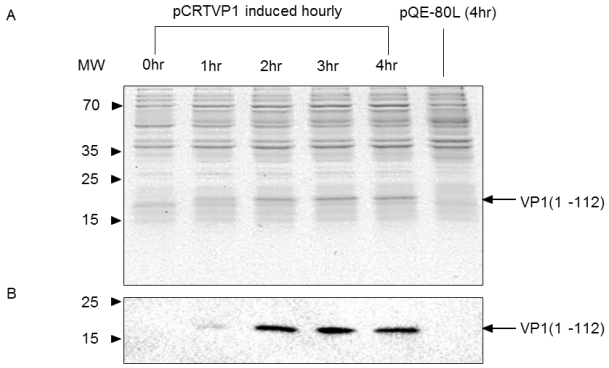

Fig. 4

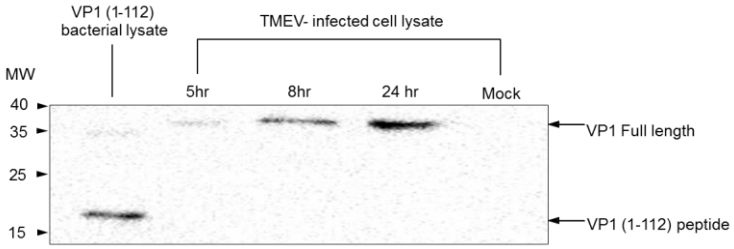

Fig. 5

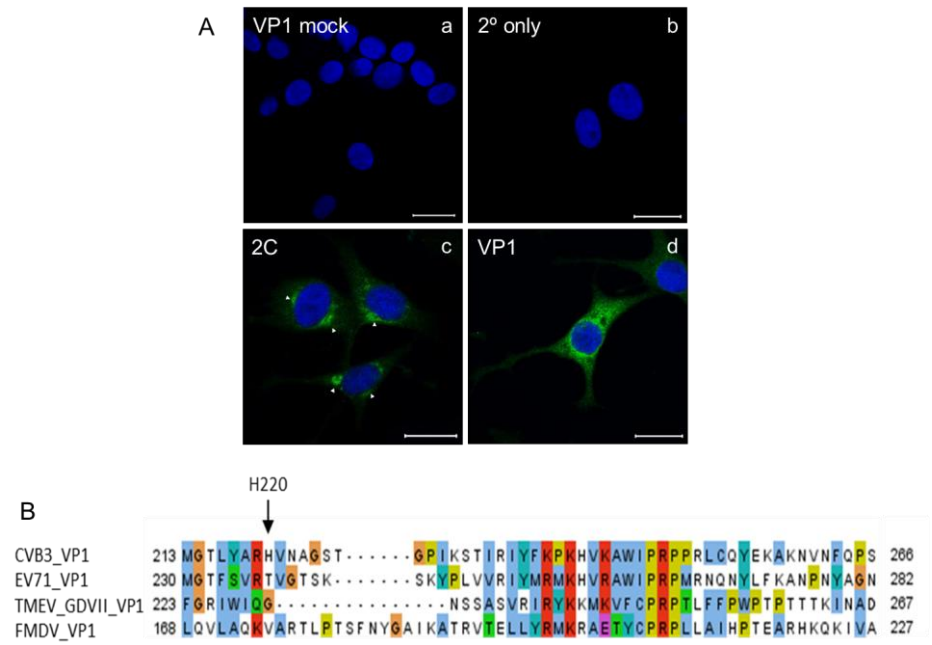

Fig. 6

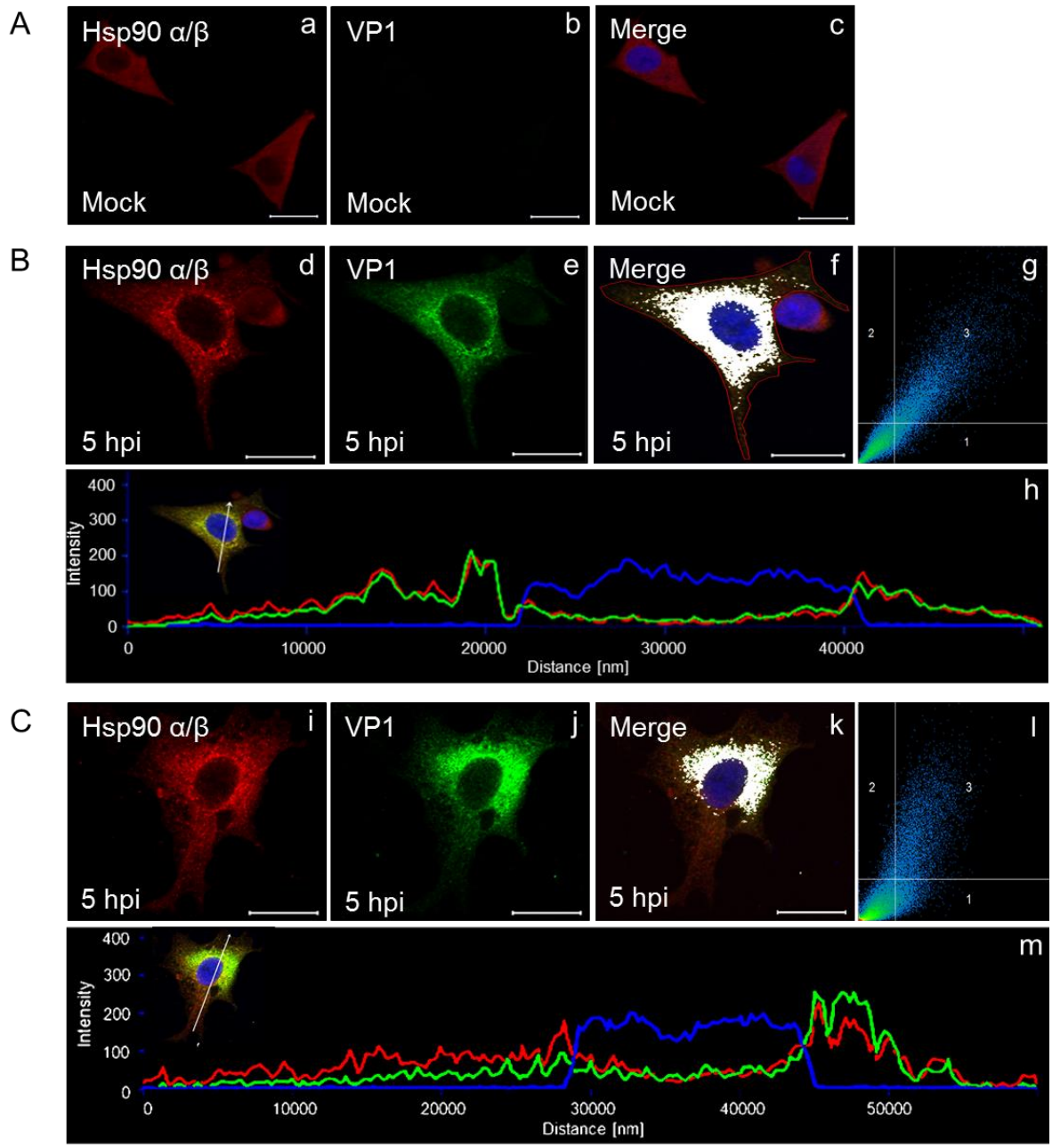

Fig. 7